J Incl Phenom Macrocycl Chem (2013) 76:75–85
DOI 10.1007/s10847-012-0175-z

ORIGINAL ARTICLE

Physical properties and inclusion interactions of new stilbazolium salts: experimental versus theoretical study

Cornelia Stolle · Bojidarka Ivanova · Michael Spiteller

Received: 3 October 2011 / Accepted: 3 May 2012 / Published online: 20 June 2012
© Springer Science+Business Media B.V. 2012

Abstract The experimental and theoretical spectroscopic and spectrometric elucidation in solid-state and gas-phase on the interacting ionic species of applied oriented synthetic derivatives on the base of the stilbazolium salts as molecular template was reported. The correlation between the molecular structure, and vibrational properties within THz-regime (10-0.3 THz) was performed. The collective vibrations, and gas-phase stabilized ionic species were comprehensive studied by the Raman spectroscopy and matrix-assisted laser desorption/ionization mass spectrometry, using the embedded organic dyes in host matrixes. The performed solid-state quantum chemical calculations contributed to further understanding of the nature of the guest–host interacting systems as well as to explain the observed optical phenomena within the THz-region.

Keywords Matrix-embedded organic dyes · Physical properties · Mass spectrometry · Quantum chemistry

Introduction

Considerable interest, recently, in organic non-linear optical (NLO) materials has been based on the discoveries on their THz-generation properties and application in the THz technologies [1–21]. The highly interdisciplinary nature of this field is striking, shaping collaborations in the fields of space communications, security, materials analysis, environmental inspection and detection, human healt, socia science, and more [22–25]. Particularly interesting amount the organic materials were found, the organic dyes [1–27], characterizing with the tunable D-π-A, π-conjugated core, allowing both experimental and theoretical modelling the D- and A-substitutions in respect their electronic and molecular structure, effecting in significant level of the electronic transitions in the frame of the conjugated core. Additional advantages, as for example, high chromophore number density and excellent long-term orientation stability compared to poled polymers marked all studied derivatives as promising THz-materials. The 4-*N*,*N*-dimethylamino-4′-*N*′-methyl-stilbazolium tosylate (DAST) was shown to exhibit pronounced bulk second-order NLO activity with a powder SHG efficiency 1.10^3 times that of the urea standard at 1,907 nm [28, 29]. Moreover, the molecular architecture the DAST has the possibility for further design, using the molecular and crystal engineering strategies. Since, the THz-properties were associated with a kind charge transfer (CT) such as intramolecular electron transfer between donor and acceptor the physical characteristic as the large first hyperpolarizabilities β, governing second order NLO effects, were generally require at the molecular level. In terms the crystal engineering, the noncentrosymmetric crystals, defining the NLO bulk response, χ^2, were obtained by tuning of the self-assembly and packing of individual molecules, design the Coulomb interactions, by charged chromophores in a combination with counter-ions and/or using of a relatively flexible π-conjugated core. Thus, organic dyes appeared promising templates for the applied oriented synthesis of novel THz-materials [1–31]. Since, the Raman spectroscopy, was amounth the phundamental methods for study the optical phenomena both of isolated molecules as well as of the ensemble of interacting species in solids, including crystalline state, the paper highlighted the advantages the method for study the molecular vibrations within the 10-0.3 THz of series of substituted dyes, based on

C. Stolle · B. Ivanova (✉) · M. Spiteller
Institut für Umweltforschung, Universität Dortmund,
Otto-Hahn-Strasse 6, 44221 Dortmund, Germany
e-mail: B.Ivanova@infu.uni-dortmund.de

the stilbazolium salts as molecxular template. The obtained theoretical β and χ^2 values, 2.1–3.4 times higher than DAST, using as standard, marked reported materials as attractive objects for THz technologies. Moreover the reported findings shaped the multidisciplinarity of the interest, including Raman, far-IR and THz-spectroscopy. Since, the molecular interactions of the studied systems specified as well the physical phenomena in gas-phase, through the stabilized dyes-matrixes ionic species, they involved advanced mass spectrometric (MS) methods such as matrix-assisted laser desorption/ionization (MALDI)-Orbitrap MS spectrometry, as fundamental one provided experimental evidence about the nature of these interactions.

Experimental

Physical methods

The powder X-day diffraction measurements were carried out on polycrystalline and/or glass samples. The XRD patterns were obtained using a Rigaku MiniFlex powder diffraction system, equipped with a horizontal goniometer in the $\theta/2\text{-}\theta$ mode. The X-ray source was nickel-filtered K-α emission of copper (1.54056 Å). Samples were packed into an aluminium holder using a back-fill procedure and will be scanned over the range of 50–6° 2-θ, at a scan rate of 0.5° 2-θ/min. Using a data acquisition rate of 1 point per second, the scanning parameters equate to a step size of 0.0084 degrees 2-θ. Calibration of each powder pattern will be effected using the characteristic scattering peaks of aluminum at 44.738 and 38.472° 2-θ. Conventional IR and Raman spectroscopy in solid-state were performed on a Thermo Nicolet 6700 FTIR spectrometer (4,000–400 cm^{-1} region, resolution 0.5 cm^{-1} and 100 scans), and a NXR FT-Raman module within the 4,000–50 cm^{-1} region. The UV–Vis–NIR spectra between 190 and 1,190 nm, using solvent acetonitrile (Uvasol, Merck product) at a concentration of $2.5.10^{-5}$ M in 0.921 cm quartz cells were recorded on Tecan Safire Absorbance/Fluorescence XFluor 4 V 4.40 spectrophotometer. The thermo gravimetric study was carried out using a Perkin-Elmer TGS2 instrument. The calorimetric measurements were performed on a DSC-2C Perkin Elmer apparatus under argon. Solid-state UV–Vis spectra were measured on a PerkinElmer Lambda 750 in reflectance mode. The reflection spectra were automatically converted to absorbance spectra using Kubelka–Munk theory. ^{1}H and ^{13}C-NMR spectra were obtained at Bruker 400 XC spectrometer, using TMS as standard in CD_3OD. The analyses of the samples by ESI mass spectrometry were performed with a Thermo Finnigan surveyor LC-Pump. Compounds were separated on a Luna C18 column (150 × 2 mm, 4 μm particle size) from Phenomenex (Torrance, CA, USA), using a gradient program.

HPLC–MS/MS measurements were made using TSQ 7000 instrument (Thermo Electron Corporation). Two mobile phase compositions were used: (A) 0.1 % v/v aqueous HCOOH and (B) 0.1 % v/v HCOOH in CH_3CN. Electrospray ionization (ESI) mass spectrometry. A triple quadrupole mass spectrometer (TSQ 7000 Thermo Electron, Dreieich, Germany) equipped with an ESI 2 source was used and operated at the following conditions: capillary temperature 180 °C; sheath gas 60 psi, corona 4.5 μA and spray voltage 4.5 kV. Sample was dissolved in acetonitrile (1 mg ml^{-1}) and was injected in the ion source by an autosampler (Surveyor) with a flow of pure acetonitrile (0.2 ml min^{-1}). Data processing was performed by Excalibur 1.4 software.

A standard LTQ Orbitrap XL instrument is used for the MALDI MS measurements, using the UV laser source at 337 nm. An overall mass range of m/z 100–1,000 is scanned simultaneously in the Orbitrap analyzer. The samples are measures in solid state, using a variant of the spray technique of solution, containing the matrix and analyte compound. The solution of thus, obtained thin liquid films is fast evaporated to formation of the sample of matrix/matrix/analyte embedded samples. The habitus of the crystals depends strongly of the crystallographic space system. Under these conditions however the obtained polycrystalline samples are characterized with the relatively small crystal size, increasing the quality of the obtained spectra. The 2,5-dihydroxy benzoic acid (DHB) was used as matrix.

Computational details

Quantum chemical calculations were performed with GAUSSIAN 09 and Dalton 2.0 program packages [32, 33], visualizing by GausView03 program package [34]. The geometries of the studied species were preoptimized employing B3LYP method, CAM-B3LYP, and M06-2X functionals [35, 36]. Molecular geometries of the studied species were fully optimized by the methods and algorithms described in [17, 18, 37–42]. The calculations of the molecular vibrations were utilized by the 6-31+G(d,p) and aug-cc-pVDZ basis set. The obtained vibrational characteristics, by the preliminary optimization of the molecular geometry are correlated to those, obtained by the crystallographic inputs according the method described in [17, 18, 43–47]. The UV–Vis spectra were calculated, using TDDFT method as above levels and PCM approach [35–42].

Statistical methods

The experimetal and theoretical spectroscopic patterns were processed by R4Cal OpenOffice STATISTICs for Windows

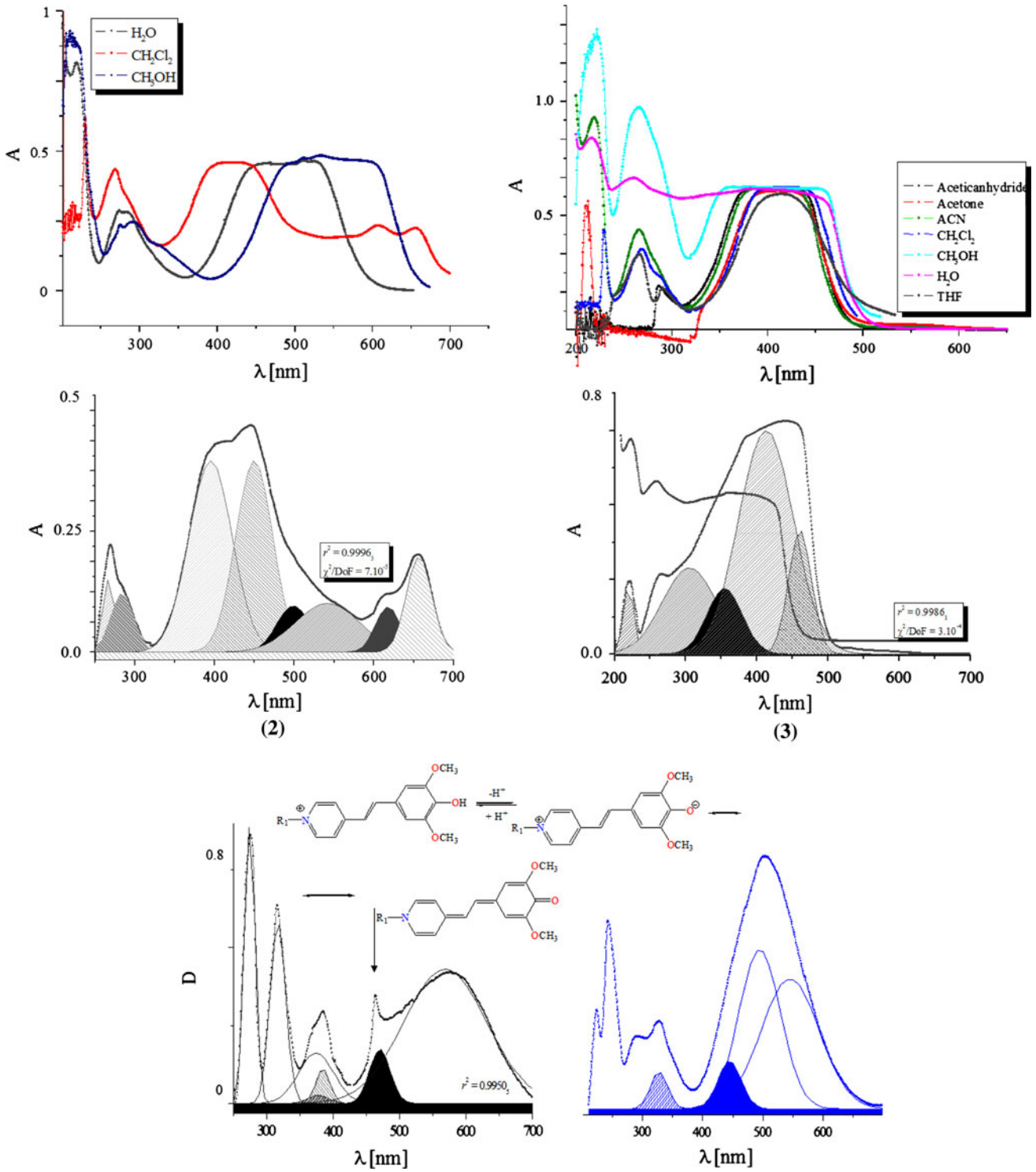

Fig. 1 Electronic absorption (*A*) spectra of studied dyes in solution depending of the solvent polarity at concentrations 2.10^{-4} mol/l and 1 cm quartz cell; diffuse reflectance spectra in solid-state (*D*); chemical diagram of the resonance forms (aromatic and quinoide ones) depending of the pH of the medium; curve-fitted spectroscopic patterns after the baseline correction method, by non-linear multipeak Gaussian function; *A*—total area under the curve from the baseline centre of the peak; w^2 "sigma", ~0.856 the FWHM; *w*/2—is the standard deviation; statistical r^2 and χ^2/DaF values

7 program package [48]. Baseline corrections and non-linear curve-fitting procedures were applied and described in [44, 45]. The statistical significance of each regression coefficient was checked by the use of *t* test. The model fit was determined by *F* test (comparison of calculated by the model and experimentally obtained signal values) [49–51].

Synthesis

The 1-cyclohexyl-4-[2-(4-hydroxy-3,5-dimethoxy-phenyl)-vinyl]-pyridinium iodide (**2**) and 4-[2-(4-hydroxy-3,5-dimethoxy-phenyl)-vinyl]-1-methyl-pyridinium iodide (**3**) were obtained by the classical reaction scheme [52], by mixing of the equimolar ratios of the starting syringaldehyde (**1**) and corresponding 1,4-dimethyl-pyridinium iodide or 1-cyclohexyl-4-methyl-pyridinium iodide (Sigma-Aldrich products), preliminary dissolved in solvent methanol. The obtained solutions are under stirring for 5 h at 70 °C. The obtained precipitates were filtered off, washed with ethanol and dried on air at 298 K and recrystallized to the thin plate 2D crystals from solvent mixture methanol:water 1:1 (Fig. 1). (**2**), Found, C, 48.3; H, 4.55; calc. [$C_{16}H_{18}NO_3I$], C, 48.1; H, 4.5 %; ^{1}H-NMR, δ, ppm 0.9 (3H, s, N–C**H**$_3$), 3.77 (s, 6H, O–C**H**$_3$), 6.72 (m, 2H), 7.88–6.93 (m, 8H, C**H**), 9.4 (s, 1H, O**H**); ^{13}C-NMR; 56.1, 125, 127.3, 129.8, 130,2, 142.8; MS, *m/z* 272.18 $[M+1]^+$; (**3**), Found, C, 53.1; H, 5.66; calc. [$C_{21}H_{26}NO_3I$], C, 53.9; H, 5.6 %; ^{1}H-NMR, δ, ppm 1.44 (m, 10H, C**H**$_2$), 3.78 (s, 6H, O–C**H**$_3$), 6.70 (m, 2H), 7.80–6.95 (m, 8H, C**H**), 9.1 (s, 1H, O**H**); ^{13}C-NMR; 23.4–27.9, 56.0, 124, 121.1, 129.1, 130.0, 141.5; MS, *m/z* 340.5 $[M+1]^+$; respectively. The thermal methods within 200–500 K show an absence of the included solvent water molecules in (**2**) and (**3**), respectively. The powder XRD diffraction data show the triclinic space systems of both of the dyes with the unit cell dimensions of a = 10.663, b = 10.118, c = 13.982 Å; $\alpha = 94.1(7)°$, $\beta = 95.2(9)°$ and $\gamma = 111.0(5)°$ (**2**), and a = 13.271, b = 13.346, c = 15.072 Å; $\alpha = 98.2(5)°$, $\beta = 90.6(9)°$ and $\gamma = 116.3(6)°$ (**3**), respectively. The corresponding quinoide forms 4-[2-(1-methyl-1*H*-pyridin-4-ylidene)-ethylidene]-2,6-dimethoxy-cyclohexa-2,5-dienone (**2a**) and 4-[2-(1-cyclohexyl-1*H*-pyridin-4-ylidene)-ethylidene]-2,6-dimethoxy-cyclohexa-2,5-dienone (**3a**) were obtained after mixing of the compounds (**2**) or (**3**) respectively with the equimolar ratios of KOH in methanol.

Results and discussion

The theoretical optical and NLO optical properties of the functionalized dyes were summarized in Table 1. The

Table 1 Theoretical dipol moments (μ_{tot}), static polarizabilities (α_{ij}) and first hyperpolarizabilities (β_{ijk}) (a.u.) of depicted dyes (**2**) and (**3**) and their forms (**2a**) and (**3a**), depending the pH at M06-2X/aug-cc-pVDZ theoretical levels; the btot value is calculated by the $\|\beta\| = (\beta_x^2 + \beta_y^2 + \beta_z^2)^{1/2}$; theoretical data for DAST core at same level are: $\mu_{tot} = 9.813$, $\alpha_{xx} = 52.8$, $\alpha_{yy} = -86.8$, $\alpha_{zz} = -109.5$, $\beta = 403.856$, respectively

	(**2**)	(**2a**)	(**3**)	(**3a**)
μ_{tot}	21.2	24.5	22.7	25.4
α_{xx}	40.6	−81.3	−191.0	−193.2
α_{yy}	−92.3	−101.7	−111.8	−132.0
α_{zz}	−119.4	−121.2	−116.2	−152.4
α_{xy}	−8.6	0.3	−2.0	−2.4
α_{xz}	15.1	14.2	21.1	24.2
α_{yx}	3.1	0.9	−0.9	−1.8
γ_{xxxx}	−4090.5	−8082.4	−18223.2	−25316.4
γ_{yyyy}	−1530.3	−1671.3	−980.1	−1910.6
γ_{zzzz}	−231.0	−243.6	−222.7	−424.4
γ_{xxxy}	−219.6	7.1	−98.3	−197.2
γ_{xxxz}	263.4	149.5	450.1	951.7
γ_{yyyx}	14.3	33.0	17.0	35.1
γ_{yyyz}	13.0	10.9	−7.7	−14.1
γ_{zzzx}	−3.5	−1.6	1.2	2.3
β_{xxx}	−804.3	−822.3	−910.2	−967.9
β_{yyy}	−2.0	1.9	10.1	12.4
β_{zzz}	−1.5	3.5	1.2	0.9
β_{xyy}	−21.0	−29.6	5.7	6.2
β_{xxy}	−77.9	−30.7	−10.1	−13.3
β_{xxz}	49.0	97.9	170.0	175.1
β_{yzz}	9.5	13.7	−1.0	−0.6
β_{yzz}	−2.0	0.1	−1.5	−4.0
β_{yyz}	28.4	30.1	25.1	29.5
β_{xyz}	−3.1	−1.7	0.2	1.5
γ_{zzzy}	−1.3	−0.5	−0.1	−1.1
γ_{xxyy}	−1624.6	−1748.8	−1567.5	−3799.7
γ_{xxzz}	−1883.8	−1847.7	−2509.1	−3857.6
γ_{yyzz}	−332.5	−352.1	−222.5	−424.7
γ_{xxyz}	47.9	−17.5	−18.2	−32.9
γ_{yyxz}	111.8	106.5	77.8	158.7
γ_{zzxy}	−16.5	−0.4	−6.1	−10.2

Table 2 Theoretical (M06-2X/aug-cc-pVDZ) and experimental electronic absorption spectra of (**2**) and (**3**), as well as corresponding quinoide forms (**2a**) and (**3a**), respectively, λ (nm) (f); solid-state electronic absorption spectra of the molecular dimeric species labels as in Fig. 4, obtained after the preoptimization of the geometry at CAM-B3LYP/6-31+G(d,p) level of theory

(**2**)	(**2a**)	(**3**)	(**3a**)	(**2**) Dimer (a)	(**2**) Dimer (b)	(**3**) Dimer (a)	(**3**) Dimer (b)
382.4 (0.858)	433.4 (1.398)	408.2 (0.981)	436.5 (1.562)	398.9 (1.772)	381.2 (0.888)	444.1 (0.981)	410.7 (1.271)
330.4 (0.003)	387.2 (0.000)	337.2 (0.022)	384.4 (0.000)	339.1 (0.231)	331.2 (0.010)	385.1 (0.271)	333.1 (0.222)
286.0 (0.001)	348.5 (0.025)	325.2 (0.028)	347.9 (0.015)	290.0 (0.226)	285.1 (0.088)	355.2 (0.271)	344.1 (0.133)

obtained values of the aromatic forms of the dyes were correlated to the quinoide forms, stabilized in solution depending of the pH (Fig. 1). The theoretical and experimental optical properties (Tables 1, 2) showed a good correlation of about 3 nm for the predicted absorption maxima, thus assuming the precise calculation of the NLO properties. The negative solvatochromism of about 263 nm is obtained for (**3**) depending of the solvent polarity, appeared one of the highest reported values in the literature [1–28]. Significantly contributed to the obtained value, the cyclohexyl substituent at R_1-position and the syringaldehyde fragment [1–28]. The solvatochromic effect for (**2**) was smaller that the (**3**) at same experimental conditions and was obtained of about 60 nm. Nevertheless the reported data were about three times higher than those, of the classical NLO materials of the stilbazolium (resp. merocyanine) type. The effect was strongly associated with the intramolecular CT, illustrated by the localized HOMO and LUMO gaps within the frame of the planar aromatic skeletal of the studied dyes (Scheme 1), and obtained at same theoretical levels. The values were higher of about 30 nm to those for derivative with R_1 = butyl [53]. The presence of the multicomponent maxima within 600–700 nm of (**2**) in CH_2Cl_2 was an indication of the H-types aggregation, typical for merocyanine dyes [54–63]. The absence of such aggregates in (**3**), could explain with the bulk substituent in the R_1-position. Since, the solid-state spectra were characterised with the typical spectroscopic of isolated dyes (Fig. 1) as well, a molecular orientation of the interacted species for the noncentro symmetric crystals of dyes (Fig. 4) with $Z = 2$ was expected. The precise vibrational assignment of (**2**) and (**3**), was supported by the study of the vibrations of syringaldehide moiety (**1**). A parallel between the Raman spectroscopic data and the hydrogen bonding effects in the structure of (**1**) was performed, using our crystallographic data [58]. The (**1**), crystalized centrosymmetrically in monoclinic space system and $P2_1/n$ space group. The unit cell contained four molecules (Fig. 2), forming infinite chains by only one type intermolecular interaction in the terms of the classical "hydrogen bonds". In parallel, the series of short contacts were observed (Table 2). The molecular crystal of (**1**) allowed to test new theoretical approaches, consisted of the optical study of isolated molecule, two types of dimer associates as well as full set of observed molecules in the unit cell (Fig. 2). Thus, for the relatively small interacting molecules, of mainly 1D and 2D crystals with limited number of the hydrogen bonding scheme and molecular flexibility, the optical phenomena and structure appeared theoretically predictable at the high level of the confidence. The obtained theoretical electronic absorption spectra in solution, provided an evidence about the successful theoretical model, giving a difference of 2 nm of the predicted spectra in condense phase (Fig. 1). Promising were found as well the predicted vibrational properties of the molecular ensemble of interacted species (Fig. 3). The typical vibrations of the quinoide form of the dyes were found within 1,700–400 cm^{-1} and well as 900–400 cm^{-1}, regions, while those of the stilbazolium salts, both IR- and Raman active modes were observed at about 1,643 (**8a**), 1,626 (**8b**), 1,600 (**19a**), 1,476 cm^{-1} (**19b**) as well as 836 cm^{-1} (**11**) of the in- (i.p.) and out-of-plane (o.p.) vibrations of the aromatic skeletons (Fig. 2). The IR-active bands of conjugated $\nu_{C=O}$ and $\nu_{C=C}$ bonds, the γ_{CH} o.p. modes of the *cis*-di- and *trans*-substituted double bonds were observed within 1,700–1,400 and 930–800 cm^{-1} regions. The Raman active modes were shown in Fig. 2. The

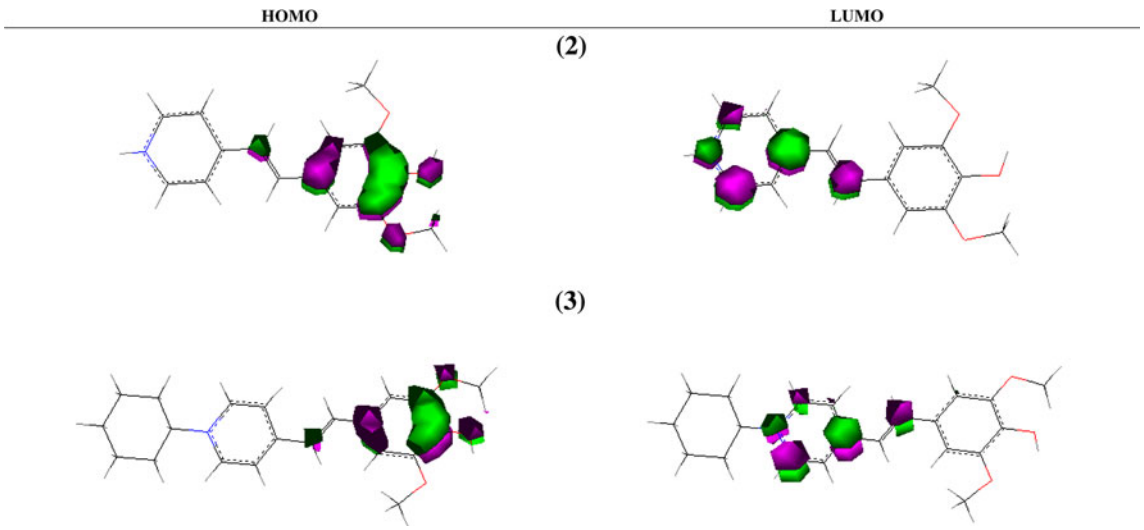

Scheme 1 HOMO-LUMO gaps of the dyes (**2**) and (**3**) at M06-2X/aug-cc-pVDZ level of theory

characteristic vibrations of the molecular ensemble of dyes in solid-state as well as this of the (**1**) within 200–30 cm^{-1} were depicted in Figs. 2, 3. The theoretical calculations of (**1**) were according the obtained centrosymmetric monoclinic space system and $P2_1/n$ space group and Z = 4. The precise localization of the protons was achieved by the low-temperature crystallographic data collection as well as high quality of the measured crystals. It is important to discussed that in contrast the prediction of the electronic absorption (resp. fluorescence [52–63]) phenomena related the electronic transitions within the frame of the aromatic conjugated systems, the theoretical prediction of the molecular vibrations in the crystals required a high quality of the crystallographic dataset used as input parameters. Thus, evaluating the error of the theoretically predicted frequencies, should take into account the error of the crystallographically determined proton positions, when were compared the experimental and theoretical modes with participation of the X–H groups (X = C, N, O, S and more). High level of confidence between the theoretical and experimentally observed solid-state vibrational spectra were achieved discussing for example the skeletal modes, where the difference between the values were fould within 1–4 cm^{-1}, respectively [17, 18, 43–46, 64, 65]. Additional evidence was found calculating (**1**) at Z = 1 (Fig. 3). The group theoretical analysis predicted two components for each of the internal modes in either the Raman or IR-spectrum 9 lattice modes, much closer to our experimental observation for the Raman spectrum of (**1**). In the case of the calculations of all four molecules, the number of

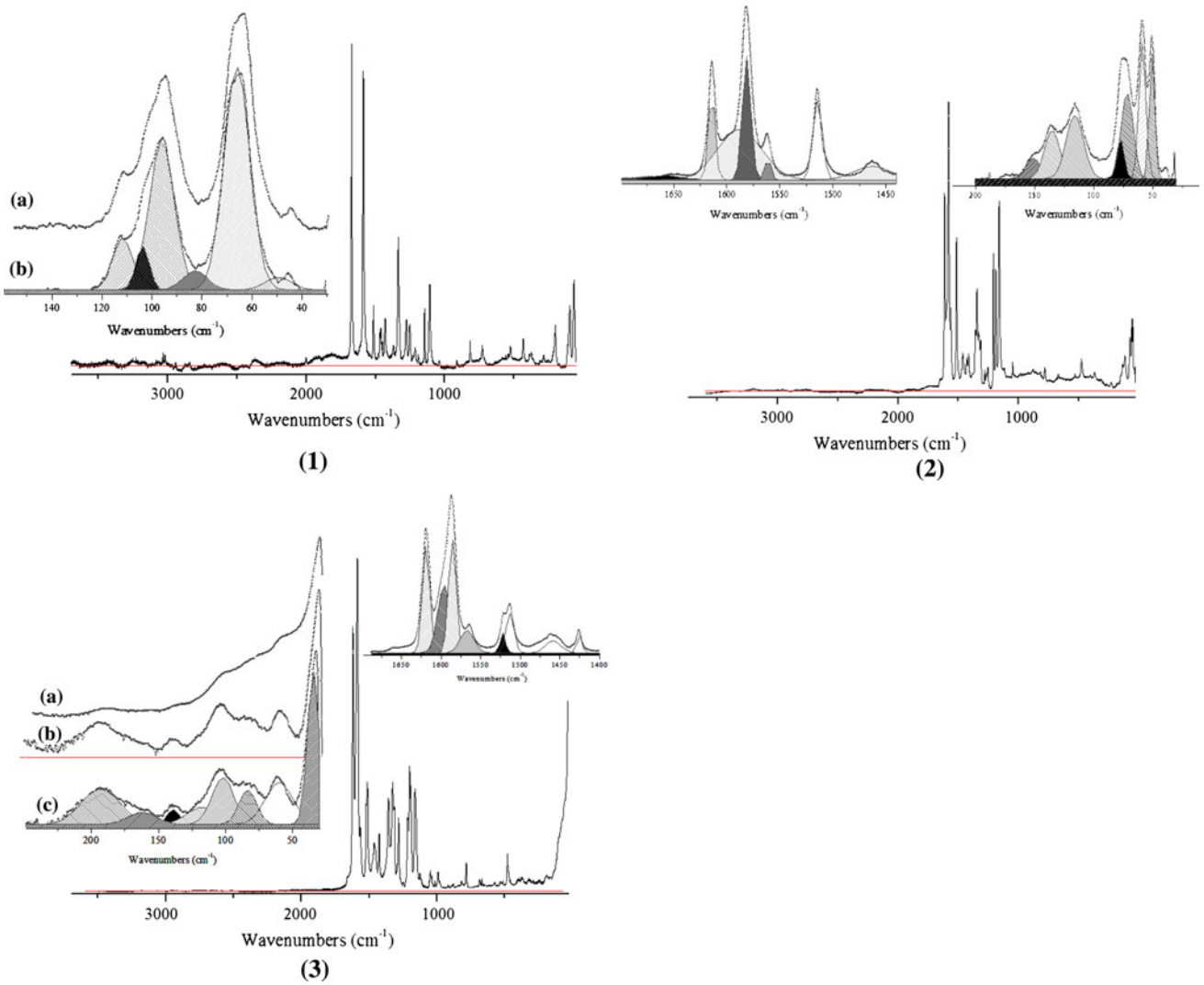

Fig. 2 Experimental solid-state Raman spectra of the syringaldehyde (**1**) and the corresponding dyes (**2**) and (**3**) within 4,000–30 cm^{-1} region; *small figures*: *a*-experimental patterns within 250–30 cm^{-1}; *b*-spectral curve, procedured with the baseline method; *b*, *c*-non-linear curve-fitted pattern after the applied deconvolution method; The corresponding r^2 (χ^2/DaF) statistical values are 0.9921_3 ($2.3.10^{-3}$) (**1**), 0.9914_2 ($2.1.10^{-3}$) (**2**) and 0.99543_6 ($1.7.10^{-4}$) (**3**), respectively

expected optical lattice modes was 21, of which 12 are Raman- and 9 IR-active. The obtained spectroscopic pattern of (**1**) within 200–30 cm^{-1}, correlated to the shown interacting species of dimers. In this case the spectroscopic patterns represented a superposition, moreover in (**1**) was found only one type of intermolecular interactions in the terms of classical hydrogen bond (OH···O, 2.714 Å). The observed LO-TO splitting of the bands was illustrated by the application of the curve-fitting and the deconvolution procedures after the preliminary baseline correction (Fig. 3). The application of the same procedures to the spectroscopic patterns of (**2**) and (**3**) within 200–30 cm^{-1} revealed series of maxima, where the number of the observed Raman bands correlated well to the triclinic *P* space system. The obtained good correlation between the theoretical and experimental Raman spectra in the same

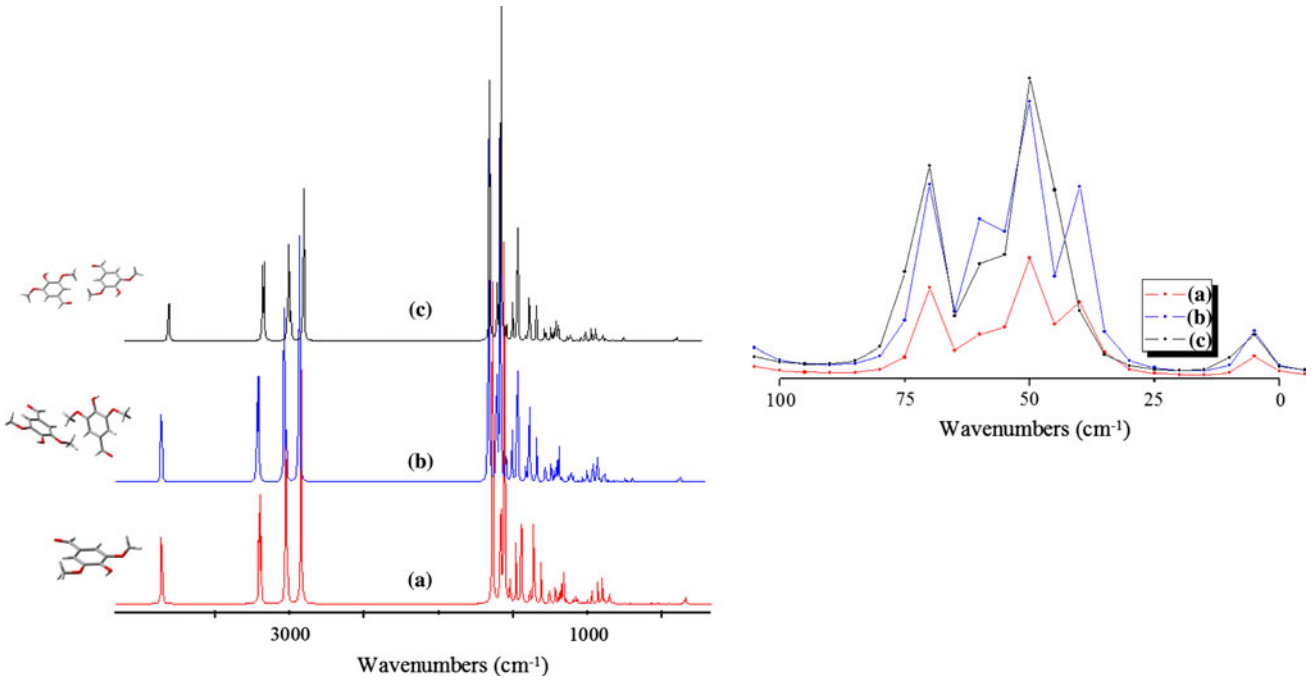

Fig. 3 Theoretical solid-state Raman spectra of the syringaldehyde (**1**) within 4,000–30 cm^{-1} region; molecular structures of the calculated species. For (**1**), are sown the calculated isolated molecule, the two dimers, obtained crystallographically in the asymmetric units and the four molecules, in the unit cell

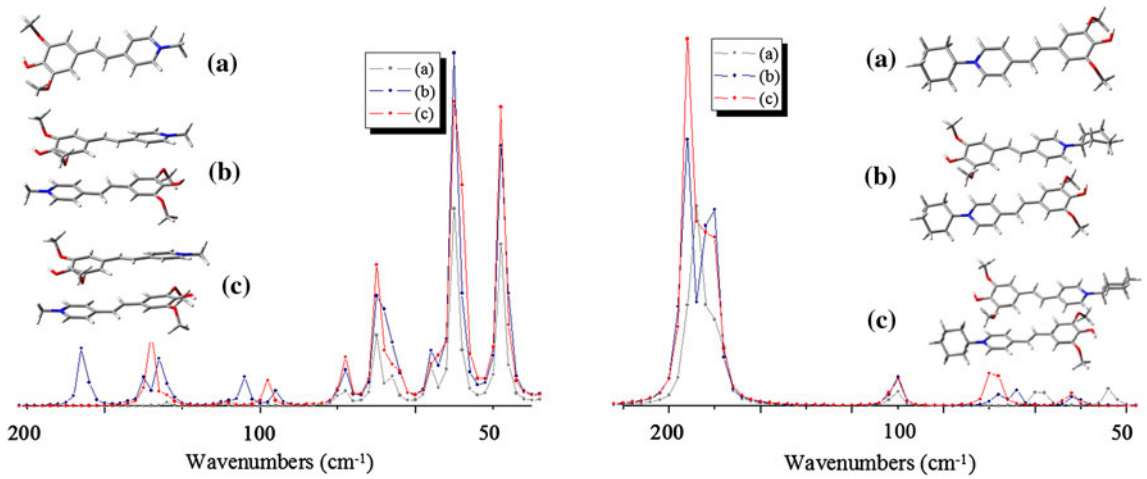

Fig. 4 Theoretical and experimental solid-state Raman spectra of the dyes (**2**) and (**3**) within 200–30 cm^{-1} region; molecular structures and orientation of the calculated species; the molecular structures of (**2**) and (**3**) are obtained by preoptimization of the geometry M06-2X/aug-cc-pVDZ method, respectively

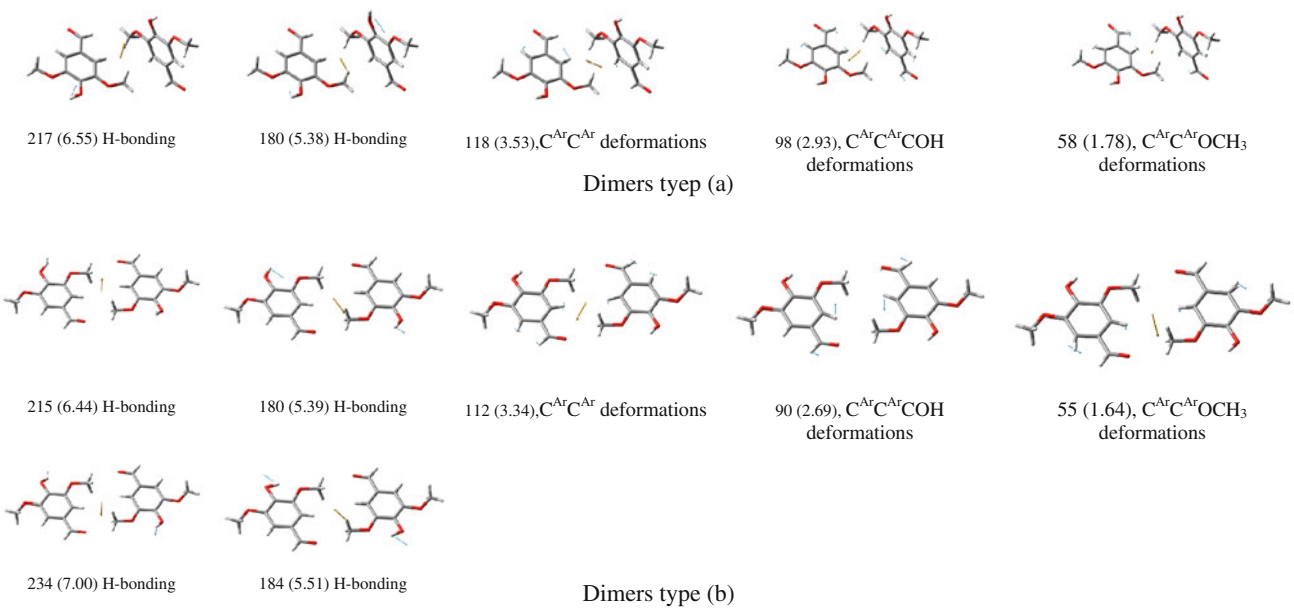

Scheme 2 Visualization of the collective vibrations of the molecules of (1), v (cm^{-1} and THz)

region, calculated for three molecules systems, i.e. isolated molecule of dye (labelled as (a) in Fig. 4), two molecules oriented in the non-centro- (b) and centrosymmetric (c) triclinic space system (Fig. 4). The data fited best to the triclinic space system and P_1 space group for (**2**) and (**3**), comparing the curves (b) in Figs. 3, 4, respectively. The obtained data from the powder XRD about the unit cells of both the dyes (**2**) and (**3**), support additionally these conclusions, where the unit cell dimensions of the polycrystalline samples correspond to crystals with triclinic space system. The spectroscopic region about at 200 cm^{-1}, was dominated by broad but well defined bands, with a series of sub-maxima, of excitations assigned to the hydrogen bond deformations (Scheme 2). To the skeletal modes, lattice vibrations in the systems (**1**), dimers (a) and (b) are assigned the excitations at 120, 118, 98 and 58 cm^{-1}, respectively. In the case of dimer associate (b), the H-bond deformations are observed as pairs of vibrations at 215/234 and 180/184 cm^{-1} (Scheme 2), assigned to corresponding symmetric and asymmetric contributions. The band at 200 cm^{-1} in (**2**), corresponded to the OH···O intramolecular hydrogen bond deformation with OH···O distance of 2.786 Å. Similarly assigned frequency in (**3**) was observed at 183 cm^{-1}. In contrast the ESI–MS data giving the peaks for the cationic species of the dyes, the MALDI-Orbitrap MS method used the solid-state sample preparation techniques (Fig. 5), give the signals in gas-phase for the matrix-analyte species of embedded in the DHB dyes. The mass spectrum of (**2**) and (**3**) (Fig. 5) were characterized with the peaks at m/z 414.22 and 482.67, which could explained with the gas-phase stabilized matrix-dye non-covalent interacting species. The peaks at 272.178 and 340.662, belonged to the cations of (**2**) and (**3**), respectively. Since the DHA appeared weak acid as well as in gas-phase dominante role would have the Coulomb interactions under the ionization conditions, fundamental understanding the physical nature of the interactions of studied guest–host systems, need further systematic study, where to evaluate the type of the dyes embedded, including study on their proton accepting and donating ability, π-staking effects and more, into different matrixes according their acidic properties as well as possibilities to forms crystals of ions and/or co-crystals during the different MALDI-MS sample preparation techniques.

Conclusions

The applied oriented molecular design and synthesis of the functionalized organic dyes, using the molecular template of the stilbazolium salts as organic materials with marked NLO properties was highlighted. Comprehensively were described the molecular excitations of the isolated molecules and ensemble of interacting guest–host species both theoretically as well as experimentally studying the collective modes of the crystals within THz-regime of 10-0.3 THz by Raman spectroscopy, as well as the gas-phase stabilized dyes-matrix by the MALDI-Orbitrap MS spectrometry. Essential were the following findings: (a) organic dyes of stilbazolium type 1-cyclohexyl-4-[2-(4-hydroxy-3,5-dimethoxy-phenyl)-vinyl]-pyridinium iodide (**2**) and 4-[2-(4-hydroxy-3,5-dimethoxy-phenyl)-vinyl]-1-methyl-

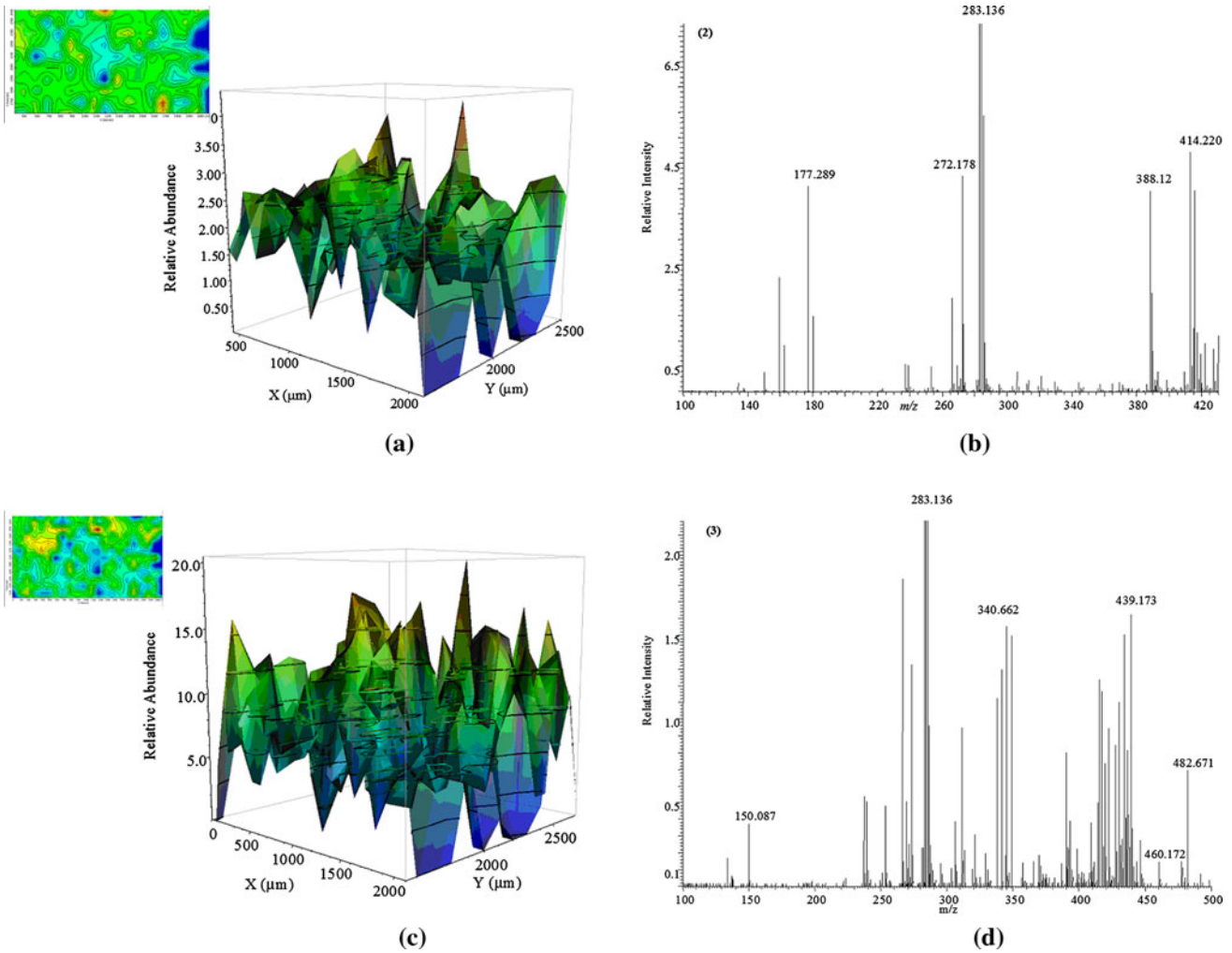

Fig. 5 3D and 2D image by logarithm plotting of Δx, Δy versus the signal amplitude (grid) of selected ion range as a function of the location of the surface for the system (**2**) and (**3**) at starting concentration of 10^{-7} mol/l of the analyte; The *scan areas*, presented as corresponding SN are shown with *circles* (*a*); corresponding mass spectra (*b*)

pyridinium iodide (**3**) as well as their merocyanine analogues 4-[2-(1-methyl-1*H*-pyridin-4-ylidene)-ethylidene]-2,6-dimethoxy-cyclohexa-2,5-dienone (**2a**) and 4-[2-(1-cyclohexyl-1*H*-pyridin-4-ylidene)-ethylidene]-2,6-dimethoxy-cyclohexa-2,5-dienone (**3a**), were characterized with the first molecular hyperpolarizability β_{tot}, higher than the DAST core; (ii) The XRD data of the thin 2D crystals showed triclinic space system and unit cell parameters, a = 10.663, b = 10.118, c = 13.982 Å; $\alpha = 94.1(7)°$, $\beta = 95.2(9)°$ and $\gamma = 111.0(5)°$ (**2**), and a = 13.271, b = 13.346, c = 15.072 Å; $\alpha = 98.2(5)°$, $\beta = 90.6(9)°$ and $\gamma = 116.3(6)°$ (**3**), respectively; (iii) The spectroscopic region within 200–180 cm^{-1}, was dominated by a broad but well defined bands, with a series of sub-maxima of excitations assigned to the inter- and intramolecular hydrogen bond deformations of OH···O bonds. To the skeletal modes, and lattice vibrations are assigned the vibrations within 120–30 cm^{-1}, respectively. The theoretical vibrational solid-state calculations of triclinic systems of dyes and Z = 2 in non- and centrosymmetric P_1 and P-1 space groups fitted best to the experimental data in the case of staked dimers; (iv) The theoretical method was tested, additionally for prediction of the molecular vibrations of the monoclinic space system and centro symmetric space group $P2_1/n$. (v) The performed MALDI-Orbitrap MS study of the solid-state samples of the dyes embedded in the organic matrix of DHB, provide information about the gas-phase stabilized species. The nature of the proposed non covalent forces provided fruitful area for further systematic study needed for fundamental understanding of the nature of forces, depending of the proton accepting and donating ability of the guest molecules, the possibility to form π-staking ensembles, tuning the Coulomb interactions, the acidic properties of the most molecules, possibilities to forms co-crystals during the different MALDI-MS sample preparation techniques, and more.

Acknowledgments The authors thank the *Deutscher Akademischer Austausch Dienst* (*DAAD*), for a grant within the priority program "Stability Pact South-Eastern Europe" and gratefully thank the Deutsche Forschungsgemeinschaft (DFG) for Grants SPP 255/21-1 and SPP/22-1. The authors also thank the central instrumental laboratories for structural analysis at Technical University Dortmund (TUD, Germany) and the analytical and computational laboratories at the Institute of Environmental Research (INFU) at the TUD.

References

1. Bosshard, Ch., Hulliger, J., Florsheimer, M., Günter, P.: Organic Nonlinear Optical Materials, Advances in Nonlinear Optics. Gordon and Breach Science Publishers S.A., Basel (1993)
2. Zyss, J. (ed.): Molecular Nonlinear Optics: Material Physics and Devices, Chap 4. Academic Press INC, San Diego (1993)
3. Nalwa, H., Watanabe, T., Miyata, S. (eds.): Nonlinear Optics of Organic Molecules and Polymers, p. 89. CRC Press, Boca Raton (1997)
4. Coe, B.: Switchable nonlinear optical metallochromophores with pyridinium electron acceptor groups. Acc. Chem. Rev. **39**, 383 (2006)
5. Reetz, M., Hoger, S., Harris, K.: Proton-transfer-dependent reversible phase changes in the 4,4′-bipyridinium salt of squaric acid. Angew. Chem. Int. Ed. **33**, 181 (1994)
6. Würthner, F., Schmidt, J., Stolte, M., Wortmann, R.: Hydrogen-bond-directed head-to-tail orientation of dipolar merocyanine dyes: A strategy for the design of electrooptical materials. Angew. Chem. Int. Ed. **45**, 3842 (2006)
7. Wolff, J., Wortmann, R.: Organic materials for second-order nonlinear optics. Adv. Phys. Org. Chem. **32**, 121 (1999)
8. Marder, S., Perry, J., Schaefer, W.: Synthesis of organic salts with large second-order optical nonlinearities. Science **245**, 626 (1989)
9. Papadopoulos, M., Leszczynski, J., Sadlej, J.: Nonlinear Optical Properties of Matter: From Molecules to a Condensed Phases. Kluwer, Dordrecht (2006)
10. Coe, B., Fielden, J., Foxon, S., Harris, J., Helliwell, M., Brunschwig, B., Asselberghs, C.I., Garin, J., Orduna, J.: Diquat derivatives: Highly active, two-dimensional nonlinear optical chromophores with potential redox switchability. J. Am. Chem. Soc. **132**, 10498 (2010)
11. Wampler, R., Moad, A., Moad, C., Heiland, R., Simpson, G.: Visual methods for interpreting optical nonlinearity at the molecular level. Acc. Chem. Res. **40**, 953 (2007)
12. Sullivan, P., Dalton, L.: Theory-inspired development of organic electro-optic materials. Acc. Chem. Res. **43**, 10 (2010)
13. Ward, M.: Chemistry: Molecular socks in a drawer. Nature **449**, 149 (2007)
14. Haag, R., Vögtle, F.: Highly branched macromolecules at the interface of chemistry, biology, physics, and medicine. Angew. Chem. Int. Ed. **43**, 272 (2004)
15. Holman, K., Pivovar, A., Ward, M.: Engineering crystal symmetry and polar order in molecular host frameworks. Science **2001**, 294 (1907)
16. Goodson III, T.: Optical excitations in organic dendrimers investigated by time-resolved and nonlinear optical spectroscopy. Acc. Chem. Res. **38**, 99 (2005)
17. Ivanova, B., Spiteller, M.: Noncentrosymmetric crystals with marked nonlinear optical properties. J. Phys. Chem. A **114**, 5099 (2010)
18. Ivanova, B., Spiteller, M.: Possible application of the organic barbiturates as NLO materials. Cryst. Growth Des. **10**, 2470 (2010)
19. Inerbaev, T., Gu, F., Mizuseki, H., Kawasoe, Y.: Theoretical study of solvent effect on the structure, first electronic excited state, and nonlinear optical properties of substituted stilbazolium cations. Int. J. Quant. Chem. **111**, 780 (2011)
20. Jaquemin, D., Perpete, E., Cioini, I., Adamo, C.: Accurate simulation of optical properties in dyes. Acc. Chem. Res. **42**, 326 (2009)
21. Zhao, Y., Fu, F., Peng, H., Ma, Y., Liao, Q., Yao, J.: Construction and optoelectronic properties of organic one-dimensional nanostructures. Acc. Chem. Res. **43**, 409 (2010)
22. Kang, H., Facchetti, A., Zhu, P., Jiang, H., Yang, Y., Cariati, E., Righetto, S., Ugo, P., Zuccaccia, C., Macchioni, A., Stern, C., Liu, Z., Ho, S., Marks, J.: Exceptional molecular hyperpolarizabilities in twisted π-electron system chromophores. Angew. Chem. Int. Ed. **44**, 7922 (2005)
23. Hrobarik, P., Sigmundova, I., Zahradnık, P., Kasak, P., Arion, V., Franz, E., Clays, K.: Molecular engineering of benzothiazolium salts with large quadratic hyperpolarizabilities: Can auxiliary electron-withdrawing groups enhance nonlinear optical responses? J. Phys. Chem. C **114**, 22289 (2010)
24. Pan, F., Wong, M., Gramlich, V., Bosshard, Ch., Günter, P.: A novel and perfectly aligned highly electro-optic organic cocrystal of a merocyanine dye and 2,4-dihydroxybenzaldehyde. J. Am. Chem. Soc. **118**, 6315 (1996)
25. Yang, Z., Wörle, M., Mutter, L., Jazbinsek, M., Günter, P.: Synthesis, crystal structure, and second-order nonlinear optical properties of new stilbazolium salts. Cryst. Growth Des. **7**, 83 (2006)
26. Pan, F., Wong, M., Bosshard, Ch., Günter, P.: Crystal growth and characterization of the organic salt 4-*N*,*N*-dimethylamino-4′-*N*-methyl-stilbazolium tosylate (dast). Adv. Mater. **8**, 592 (1996)
27. Adachi, H., Takahashi, Y., Yabuzaki, J., Mori, Y., Sasaki, T.: J. Cryst. Growth **198**(199), 568 (1999)
28. Okada, S., Masaki, A., Matsuda, H., Nakanishi, H., Kato, M., Muramatsu, R., Otsuka, M.: Organic salts with large second-order optical nonlinearities. Jpn. J. Appl. Phys. **29**, 1112 (1990)
29. Coe, B., Harris, J., Asselberghs, I., Wostyn, K., Clays, K., Persoons, A., Brunschwig, B., Coles, S., Gelbrich, T., Light, M., Hursthouse, M., Nakatani, M.: Quadratic optical nonlinearities of *N*-methyl and *N*-aryl pyridinium salts. Adv. Funct. Mater. **13**, 347 (2003)
30. Soegiarto, A., Comotti, A., Ward, M.: Controlled orientation of polyconjugated guest molecules in tunable host cavities. J. Am. Chem. Soc. **132**, 14603 (2010)
31. Lamshoeft, M., Storp, J., Ivanova, B., Spiteller, M.: Structural and spectroscopic study of novel Ag(I) metal-organic complexes with dyes—experimental vs. theoretical methods. Inorg. Chim. Acta **382**, 96 (2012)
32. Frisch, M., Trucks G., Schlegel, H., Scuseria, G., Robb, M., Cheeseman, J., Zakrzewski, V., Montgomery, Jr. J., Stratmann, R., Burant, J., Dapprich, S., Millam, J., Daniels, A., Kudin, K., Strain, M., Farkas, O., Tomasi, J., Barone, V., Cossi, M., Cammi, R., Mennucci, B., Pomelli, C., Adamo, C., Clifford, S., Ochterski, J., Petersson, G., Ayala, P., Cui, Q., Morokuma, K., Malick, D., Rabuck, A.D., Raghavachari, K., Foresman, J., Cioslowski, J., Ortiz, J., Stefanov, B., Liu, G., Liashenko, A., Piskorz, P., Komaromi, I., Gomperts, R., Martin, R., Fox, D., Keith, T., Al-Laham, M., Peng, C., Nanayakkara, A., Gonzalez, C., Challacombe, M., Gill, P., Johnson, B., Chen, W., Wong, M., Andres, J., Gonzalez, C., Head-Gordon, M., Replogle, E., Pople, J.: Gaussian 09, Revision A.3, Gaussian Inc., Pittsburgh (2009)
33. Dalton 2.0 Program Package. http://www.kjemi.uio.no/software/dalton/dalton.html
34. GausView03. http://www.softwarecientifico.com/paginas/gaussian.htm
35. Zhao, Y., Truhlar, D.: Density functionals with broad applicability in chemistry. Acc. Chem. Res. **41**, 157 (2008)
36. Zhao, Y., Truhlar, D.: The M06 suite of density functionals for main group thermochemistry, thermochemical kinetics, noncovalent interactions, excited states, and transition elements: Two

new functionals and systematic testing of four M06-class functionals and 12 other functionals. Theor. Chem. Acc. **120**, 215 (2008)
37. Jensen, F.: Introduction to Computational Chemistry. Wiley, New York (1999)
38. Hehre, V., Radom, L., Schleyer, P., Pople, J.: Ab Initio Molecular Orbital Theory. Wiley, New York (1986)
39. Woon, D., Dunning, T.: Gaussian basis sets for use in correlated molecular calculations. III. The atoms aluminum through argon. J. Chem. Phys. **98**, 1358 (1993)
40. Foresman, J., Head-Gordon, M., Pople, J., Frisch, M.: Toward a systematic molecular orbital theory for excited states. J. Phys. Chem. **96**, 135 (1992)
41. Wiberg, K., Hadad, C., Foresman, J., Chupka, W.: Electronically excited states of ethylene. J. Phys. Chem. **96**, 10756 (1992)
42. Bauernschmitt, R., Ahlrichs, R.: Treatment of electronic excitations within the adiabatic approximation of time dependent density functional theory. Chem. Phys. Lett. **256**, 454 (1996)
43. Ivanova, B.: Solid-state Raman spectra of non-centrosymmetric crystals—theoretical vs. experimental study towards an application in THz-regime. J. Mol. Struct. **1016**, 47 (2012)
44. Ivanova, B., Spiteller, M.: On the chemical identification and determination of flavonoids in solid-state. Talanta **94**, 9 (2012)
45. Ivanova, B., Spiteller, M.: Physical optical properties and crystal structures of organic 5-sulfosalicylates: Theoretical and experimental study. J. Mol. Struct. **1003**, 1 (2011)
46. Oppenheim, K., Korter, T., Melinger, J., Grischkowsky, D.: Solid-state density functional theory investigation of the terahertz spectra of the structural isomers 1,2-dicyanobenzene and 1,3-dicyanobenzene. J. Phys. Chem. A **114**, 12513 (2010)
47. Harsha, S., Grischkowsky, D.: Terahertz (far-infrared) characterization of tris(hydroxymethyl)aminomethane using high-resolution waveguide THz-TDS. J. Phys. Chem. A **114**, 3489 (2010)
48. http://de.openoffice.org/
49. Stephens, P., McCann, D., Cheeseman, J., Frisch, M.: Determination of absolute configurations of chiral molecules using ab initio time-dependent density functional theory calculations of optical rotation: How reliable are absolute configurations obtained for molecules with small rotations? Chirality **17**, S52 (2005)
50. Stephens, P., Devlin, F., Cheeseman, J., Frisch, M., Bortolini, O., Besse, P.: Determination of absolute configuration using ab initio calculation of optical rotation. Chirality **15**, S57 (2003)
51. Yildiz, A., Selvin, P.: Fluorescence imaging with one nanometer accuracy: Application to molecular motors. Acc. Chem. Res. **38**, 574 (2005)
52. Koleva, B., Kolev, T., Lamshöft, M., Mayer-Figge, H., Sheldrick, W., Spiteller, M.: Synthesis, spectroscopic and structural elucidation of 1-butyl-4-[2-(3,5-dimethoxy-4-hydroxyphenyl)ethenyl)] pyridinium chloride tetrahydrate. Spectrochim. Acta **74A**, 1120 (2009)
53. Dalton, G., Cifuentes, M., Petrie, S., Stranger, R., Humphrey, M., Samoc, M.: Highly Efficient Ru−Pseudohalide Catalysts for Olefin Metathesis. J. Am. Chem. Soc. **127**, 11882 (2007)
54. Kim, P., Jeong, J., Jazbinsek, M., Kwon, S., Yun, H., Kim, J., Lee, Z., Baek, I., Rotermund, F., Günter, P., Kwon, O.: Acentric nonlinear optical N-benzyl stilbazolium crystals with high environmental stability and enhanced molecular nonlinearity in solid state. Cryst. Eng. Comm. **13**, 444 (2011)
55. Würthner, F., Yao, S., Debaerdemaeker, T., Wortmann, R.: Dimerization of Merocyanine Dyes. Structural and Energetic Characterization of Dipolar Dye Aggregates and Implications for Nonlinear Optical Materials. J. Am. Chem. Soc. **124**, 9431 (2002)
56. Würthner, F., Wortmann, R., Meerholz, K.: Chromophore Design for Photorefractive Organic Materials. ChemPhysChem **3**, 17 (2002)
57. Würthner, F., Archetti, G., Schmidt, R., Kuball, H.: Solvent Effect on Color, Band Shape, and Charge-Density Distribution for Merocyanine Dyes Close to the Cyanine Limit. Angew. Chem. Int. Ed. **47**, 4529 (2008)
58. Kolev, T., Wortmann, R., Spiteller, M., Sheldrick, W., Heller, M.: 4-Hydroxy-3,5-dimethoxybenzaldehyde (syringaldehyde). Acta Cryst. **E60**, o1387 (2004)
59. Espinosa, E., Wyncke, B., Brahat, F., Gerbaux, X., Veintemillas, S., Molins, E.: Infrared vibrational spectra of L-histidinium dihydrogen orthophosphate orthophosphoric acid (LHP). Infrared Phys. Techn. **38**, 449 (1997)
60. Ohno, K., Nomura, S., Yoshida, H., Matsuura, H.: Conformational analysis of alkylamino chains using isolated C–D stretching vibrations. Spectrochim. Acta **55A**, 2231 (1999)
61. Bugueno-Hoffmann, R., Romaint, F., Pasquier, B.: Raman and far-infrared study of the polar single crystals of 3-(4-chlorophenyl)-2-cyanopropenonitrile. J. Raman Spectrosc. **19**, 101 (1988)
62. Lefebvre, J., Fontaine, H., Fouret, R.: Raman scattering of lattice vibrations in H4-urea and D4-urea. J. Raman Spectrosc. **4**, 173 (1975)
63. H Schobert, D Strauch, Investigation of the LO-TO splitting in complex binary crystals. J. Phys.: Condens. Mater. 1993, 5, 6165
64. Lamshöft, M., Storp, J., Ivanova, B., Spiteller, M.: Gas-phase CT-stabilized Ag(I) and Zn(II) metal–organic complexes—Experimental versus theoretical study. Polyhedron **30**, 2564 (2011)
65. Ivanova, B., Spiteller, M.: Ag^{I} and Zn^{II} complexes with possible application as NLO materials—Crystal structures and properties. Polyhedron **30**, 241 (2011)